RSC Advances

PAPER

View Article Online
View Journal | View Issue

Cite this: *RSC Adv.*, 2014, **4**, 46704

Structural, magnetic and dielectric properties of the Aurivillius phase $Bi_6Fe_{2-x}Mn_xTi_3O_{18}$ $(0 \leq x \leq 0.8)$

Xuzhong Zuo,[a] Jie Yang,*[a] Bin Yuan,[a] Dongpo Song,[ab] Xianwu Tang,[a] Kejun Zhang,[a] Xuebin Zhu,[a] Wenhai Song,[a] Jianming Dai*[a] and Yuping Sun[abc]

Received 9th July 2014
Accepted 9th September 2014

DOI: 10.1039/c4ra06843b

www.rsc.org/advances

The $n = 5$ Aurivillius phase ceramics $Bi_6Fe_{2-x}Mn_xTi_3O_{18}$ (BFMTO) $(0 \leq x \leq 0.8)$ were synthesized with a conventional solid-state reaction method. All samples can be indexed with an orthorhombic structure with the space group *B2cb*. The magnetic measurements indicate that these ceramics are predominantly paramagnetic with the presence of short-range antiferromagnetic interactions and a weak ferromagnetic ordering state, implying that the predicted Fe^{3+}–O–Mn^{3+} 180° ferromagnetic superexchange interaction based on the Goodenough–Kanamori rule might not be achieved in BFMTO ceramics through Mn substitution for Fe in the $n = 5$ Aurivillius phase. The dielectric loss of the $x = 0.3$ and 0.4 samples demonstrates the relaxation process and the rather large activation energy (2.63 eV for the $x = 0.3$ sample and 2.10 eV for the $x = 0.4$ sample) implies that this relaxation process is not due to the thermal motion of oxygen vacancies. The $0.5 \leq x \leq 0.8$ samples exhibit a paraelectric–ferroelectric phase transition and the ferroelectric Curie temperature decreases upon increasing the doping level of Mn.

1 Introduction

Multiferroic materials, which simultaneously exhibit magnetic, ferroelectric or ferroelastic order, have attracted much attention due to their potential device application in magnetic sensors, data storage and digital memory, *etc.*[1–3] Recently, the bismuth-based layer-structured compounds based on the Aurivillius phase[4,5] with the general formula $(Bi_2O_2)^{2+}(A_{n-1}B_nO_{3n+1})^{2-}$ (A = Na, K, Ca, Sr, Ba, Pb, Bi, *etc.*, and B = Ti, Fe, *etc.*) has been considered as one of the candidates for single-phase multiferroics by doping magnetic species at the B site into ferroelectric matrices,[6–8] where the perovskite-like layer $(A_{n-1}B_nO_{3n+1})^{2-}$ is interlayered with a fluorite-like layer $(Bi_2O_2)^{2+}$, and n refers to the layer number of the perovskite-like layers. $Bi_4Ti_3O_{12}$ has been used for nonvolatile memory because of its large spontaneous polarization and high ferroelectric Curie temperature.[9] A typical Aurivillius phase with a four-layered structure, $Bi_5FeTi_3O_{15}$ (BFTO), has been synthesized by inserting $BiFeO_3$ into a $Bi_4Ti_3O_{12}$ matrix, that exhibits weak magnetization and magnetocapacitance effect.[10,11] Some researchers found that Co-doped $Bi_5Fe_{0.5}Co_{0.5}Ti_3O_{15}$ (BFCTO) ceramic shows the coexistence of ferroelectricity (FE) and ferromagnetism (FM) above room temperature (RT).[6] Later, Yang *et al.* reported that the Nd and Co ion co-doped $Bi_{4.2}Nd_{0.8}Fe_{0.5}Co_{0.5}Ti_3O_{15}$ bulk sample presents an enhanced FM at RT.[12] Nevertheless, Keeney *et al.* argued that the magnetic origin of BFCTO may originate from the appearance of a trace amount of impurity, *i.e.*, an Fe/Co-rich spinel phase, and they found that no RT multiferroic behavior was demonstrated in Mn-doped BFTO films with $n = 4$.[13] However, RT ferromagnetism was observed in the five-layered compound $Bi_6Ti_{2.8}Fe_{1.52}Mn_{0.68}O_{18}$, in which the origin of FM was discussed according to Goodenough–Kanamori (G–K) rules.[14] Actually, it has been predicted that the Fe^{3+}–O–Mn^{3+} 180° superexchange interaction could lead to ferromagnetic interaction in Fe–O–Mn material systems. Based on the G–K rules,[15,16] many researchers have attempted to obtain FM in the Aurivillius phase. However, some failed while others have obtained the FM properties. As a result, whether the Fe^{3+}–O–Mn^{3+} 180° FM super-exchange interaction can be achieved in BTFO through the introduction of Mn at Fe sites is still an open issue. Actually, previous attempts to obtain FM in Mn-doped Aurivillius compounds mostly focused on the $n = 4$ Aurivillius phase. Systematic investigations of the magnetic and dielectric properties of Mn-doped Aurivillius compounds with $n = 5$ are still lacking. The wide disparity of magnetic properties reported in the literature for Fe–O–Mn material systems calls for more experimental studies on Aurivillius compounds with different n. Moreover, the investigations on dielectric properties in the Aurivillius phase are also important in developing engineering capacitors. Some

[a]*Key Laboratory of Materials Physics, Institute of Solid State Physics, Chinese Academy of Sciences, Hefei 230031, People's Republic of China. E-mail: jyang@issp.ac.cn; jmdai@issp.ac.cn*

[b]*University of Science and Technology of China, Hefei 230026, People's Republic of China*

[c]*High Magnetic Field Laboratory, Chinese Academy of Sciences, Hefei 230031, People's Republic of China*

researchers combined the advantages of ceramics and polymers to obtain a composite dielectric to achieve a high dielectric constant and high breakdown strength.[17,18] The doping method may be another way to enhance the dielectric properties and breakdown strength. In this paper, we have systematically investigated a series of Mn-doped samples $Bi_6Fe_{2-x}Mn_xTi_3O_{18}$ ($0 \leq x \leq 0.8$) by using the measurements of X-ray diffraction (XRD), magnetization, and dielectric constant. Our present work reports a detailed evolution of magnetic and dielectric properties in $n = 5$ Aurivillius compounds within a wide doping level of Mn. The results may provide a point of reference for understanding magnetic and dielectric properties for Mn-doped Aurivillius materials with $n = 5$.

2 Experiment

The polycrystalline ceramics $Bi_6Fe_{2-x}Mn_xTi_3O_{18}$($0 \leq x \leq 0.8$) were prepared with a conventional solid-state reaction method. Stoichiometric amounts of high purity Bi_2O_3(99.975%) (10 wt% excess to compensate for the volatilization of Bi), Ti_2O_3 (99.9%), Mn_2O_3 (99.5%), and Fe_2O_3 (99.99%) were mixed and ground, and then calcined at 600 °C for 20 h. The obtained powders were ground, pelletized, and sintered at 850 °C for 10 h with an intermediate grinding, and finally the furnace was cooled slowly to RT. The crystal structure was determined with a powder X-ray diffractometer using Cu K_α radiation at RT. A field-emission scanning electron microscope (FESEM, Sirion 200, FEI Company) was used to characterize the surface morphology of the samples. The magnetic measurements were carried out with a quantum design superconducting quantum interference device (SQUID) magnetic property measurement system (MPMS) ($2 \leq T \leq 400$ K, $0 \leq H \leq 5$ T). Dielectric constant and loss tangent were measured with a precision LCR meter (TH2828/A/S) in the frequency range of 3 kHz to 1 MHz at temperatures ranging from RT to 1000 K.

3 Results and discussion

Fig. 1(a) shows the XRD patterns of BFMTO at RT and all samples are of single-phase with no detectable secondary phases. We refined the structural parameters by using the program FULLPROF and all samples can be indexed with an orthorhombic lattice with the space group *B2cb*, which is in agreement with previous results for the five-layered Aurivillius phase.[19,20] As an example, the experimental and calculated XRD patterns of $Bi_6Fe_{1.6}Mn_{0.4}Ti_3O_{18}$ are shown in Fig. 1(b). The fit between the experimental and calculated XRD patterns is relatively good based on the consideration of the lower R_P value of 11.7. The dependence of lattice parameters on the doping level of Mn is shown in Fig. 1(c). The lattice parameters change slightly since the Mn^{3+} and Fe^{3+} ions have identical ionic radii (0.645 Å) in six-fold octahedral coordination. Fig. 2(a)–(f) show the representative FE-SEM images of BFMTO with $x = 0$, 0.2, 0.4, 0.5, 0.7, and 0.8. The samples consist of plate-like crystalline grains, which is the typical feature of layer-structured Aurivillius ceramics. Moreover, the samples have a relatively uniform and compact microstructure. Upon increasing the doping level of Mn, the plate-like grains apparently become large implying that Mn-substitution can effectively promote the grains' growth.

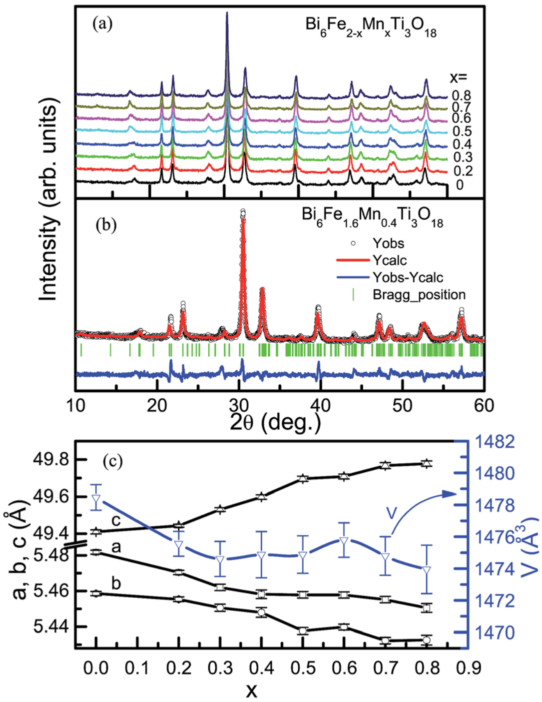

Fig. 1 (a) XRD patterns of $Bi_6Fe_{2-x}Mn_xTi_3O_{18}$ ($0 \leq x \leq 0.8$). (b) The Rietveld refinement results of $Bi_6Fe_{1.6}Mn_{0.4}Ti_3O_{18}$. Circles indicate the experimental data and the calculated data are the continuous line overlapping them. The vertical bars indicated the expected reflection positions. The lowest curve shows the difference between the experimental and calculated patterns. (c) Lattice parameters as a function of the doping level of Mn.

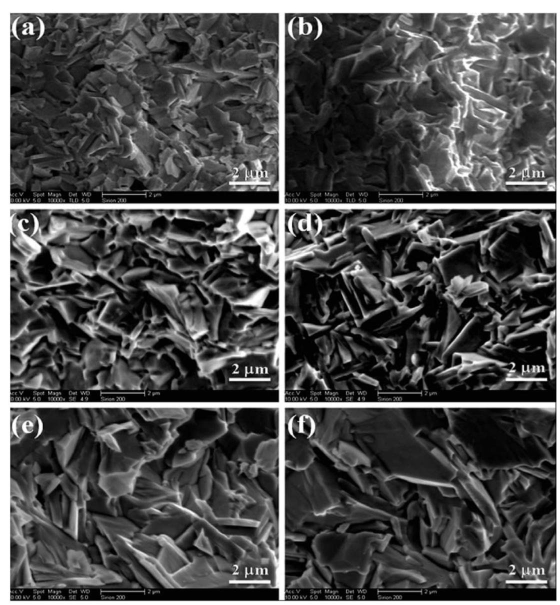

Fig. 2 Representative SEM images of $Bi_6Fe_{2-x}Mn_xTi_3O_{18}$ with (a) $x = 0$, (b) $x = 0.2$, (c) $x = 0.4$, (d) $x = 0.5$, (e) $x = 0.7$, and (f) $x = 0.8$.

The magnetization (M) *versus* temperature (T) plots of all of the samples measured at $H = 100$ Oe in the zero-field-cooled (ZFC) and field-cooled (FC) modes are shown in Fig. 3. A paramagnetic (PM)-like temperature dependence of magnetization was observed with no evidence of magnetic ordering at low temperatures due to the monotonous increase in the magnetization with decreasing temperature. For quantitative evaluation, the M–T data in FC mode are described by the modified Curie–Weiss relation:[21,22]

$$M_{\mathrm{PM}}(T, H) = [\chi_0 + C(T - \theta)]H, \tag{1}$$

where χ_0 is the temperature-independent susceptibility, the second term is the Curie–Weiss-type susceptibility, θ is the Curie–Weiss temperature, and the Curie constant $C = N\mu_{\mathrm{eff}}^2/3k_{\mathrm{B}}$ (N is the number of magnetic ions per g, μ_{eff} is the effective magnetic moment of the magnetic ion, k_{B} is the Boltzmann constant). Note that good agreement between experimental and fitting data is obtained, depicted as solid lines in Fig. 3. The very small values of χ_0 shown in Table 1 for all samples reflect a weak non-paramagnetic contribution. The negative value of θ shown in Table 1 indicates a dominant antiferromagnetic (AFM) interaction in the samples, and the absolute value of θ decreases monotonically with the increase in the doping level of Mn implying a weakening of AFM interaction upon doping with Mn, as evidenced by the linear behavior of the inverse magnetic susceptibility becoming more and more obvious with the increasing in doping level of Mn, as shown in the right panel of Fig. 3. It can be seen from Table 1 that the values of the effective magnetic moment μ_{eff} increase monotonously from 4.623(2) μ_{B} to 5.528(2) μ_{B} as x increases from 0 to 0.7 and then drops to 5.428(7) μ_{B} for $x = 0.8$. On one hand, increasing the doping level of Mn weakens the AFM interaction resulting in an increase in μ_{eff}. On the other hand, Mn^{3+} has a smaller spin quantum number $S = 2$ compared with $S = 5/2$ of Fe^{3+}, which would give rise to a decreased μ_{eff}. The former factor is dominant and μ_{eff} would increase first. A further increase in the doping level of Mn to 0.8 would render the latter factor dominant over the former and μ_{eff} would then decrease.

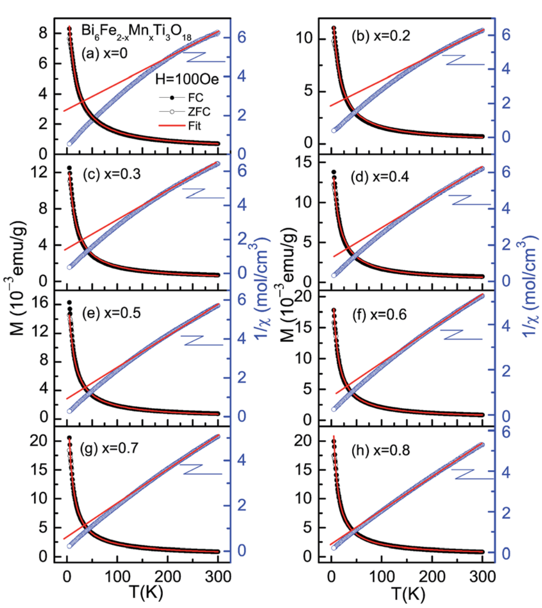

Fig. 3 Temperature dependence of magnetization in the ZFC and FC modes measured at $H = 100$ Oe and the inverse magnetic susceptibility *vs.* temperature for $Bi_6Fe_{2-x}Mn_xTi_3O_{18}$ with (a) $x = 0$, (b) $x = 0.2$, (c) $x = 0.3$, (d) $x = 0.4$, (e) $x = 0.5$, (f) $x = 0.6$, (g) $x = 0.7$, (h) $x = 0.8$. The solid lines are the fit data.

In order to make clear the magnetic behavior of BFMTO ceramics, we performed the magnetic hysteresis measurements at RT and 5 K, as shown in Fig. 4(a) and (b), respectively. The M–H curves of all samples at RT are similar and exhibit a linear behavior implying the nature of the PM state. The M–H plot at 5 K shows a different behavior compared to that at RT. Nonlinearity and a small loop indicate the existence of a weak ferromagnetic ordering in BFMTO. It is expected that there are Fe^{3+}–O–Fe^{3+}, Mn^{3+}–O–Mn^{3+}, and Fe^{3+}–O–Mn^{3+} interactions present in BFMTO. The interactions in Fe^{3+}–O–Fe^{3+} and Mn^{3+}–O–Mn^{3+} in the high spin state are AFM. Moreover, it has been predicted that the Fe^{3+}–O–Mn^{3+} 180° superexchange interaction could lead to FM interactions according to G–K rules. If the occupancy of Fe and Mn ions in BFMTO is ordered, the exchange interaction between Fe^{3+}–O–Fe^{3+} and Mn^{3+}–O–Mn^{3+} across the Bi_2O_2 layer would be long-ranged AFM and thus BFMTO would exhibit a typical AFM ground state. Actually, the Fe and Mn ions can occupy three non-equivalent positions of Ti sites in the five perovskite-like layers between the Bi_2O_2 layers and the occupancy of Fe and Mn ions in BFMTO is random with Ti ions. Therefore, no long-range AFM order would exist and instead, a local short-range AFM exists in BFMTO. Accordingly, the predicted Fe^{3+}–O–Mn^{3+} FM interactions cannot be achieved through Mn substitution for Fe in BFMTO. Furthermore, the studied samples have an orthorhombically distorted structure with a space group of *B2cb* and the distorted crystal structure with the tilted $Fe(Mn)O_6$ octahedra may give rise to canted spin structures. To the best of our knowledge, this canted spin state of two AFM coupling sublattices would favor the existence of weak ferromagnetic phases *via* the antisymmetric Dzyaloshinskii–Moriya (DM) interaction.[23,24] Actually, the canted spin structure due to DM interactions can account for the occurrence of weak ferromagnetic phases in the multiferroic perovskites.[2,3,25] As a result, the magnetic structure of BFMTO can be understood by a dominant PM state and existence of short-range AFM interactions and a weak FM ordering state. From Fig. 4(b), we note that saturated magnetization (M_{S}) increases with the doping level of Mn, which is described in detail by the field dependence of magnetization with the modified Brillouin function that is represented as:[21]

$$M = M_{\mathrm{S}}\left\{\left(\frac{2J+1}{2J}\right)\coth\left[\frac{(2J+1)y}{2J}\right] - \left(\frac{1}{2J}\right)\coth\left(\frac{y}{2J}\right)\right\} \tag{2}$$

where $y = g\mu_{\mathrm{B}}JH/k_{\mathrm{B}}(T + T_0)$, M_{S} is the saturation magnetization, μ_{B} is the Bohr magneton, g is the spectroscopic splitting factor, J denotes an average value assumed to represent the mole ratio of the high-spin of Fe^{3+} ($S = 5/2$) and Mn^{3+} ($S = 2$), and T_0 represents a measure of the interaction preventing the complete alignment of the Fe spins even at the highest field.[12] A larger T_0

Table 1 The parameters obtained from the fit of M–T and M–H data of BFMTO

Doping level of Mn	Temperature independent susceptibility χ_0 (10^{-6} emu g^{-1} Oe^{-1})	Curie–Weiss temperature θ (K)	Effective magnetic moment μ_{eff} (μ_B)	Saturation magnetization M_S (emu g^{-1})	Temperature T_0 (K)
0	2.15(2)	−12.43(1)	4.623(2)	3.00(9)	2.88(33)
0.2	1.53(8)	−8.86(2)	4.820(5)	3.42(11)	2.34(34)
0.3	0.56(6)	−8.44(2)	4.921(5)	3.98(14)	2.12(35)
0.4	0.92(5)	−7.65(4)	5.005(4)	4.03(14)	2.02(34)
0.5	1.11(7)	−6.76(2)	5.205(5)	4.70(17)	1.93(34)
0.6	1.64(4)	−6.38(1)	5.399(4)	4.86(17)	1.91(34)
0.7	1.82(3)	−5.35(3)	5.528(2)	5.38(20)	1.75(33)
0.8	1.95(4)	−5.04(1)	5.428(7)	5.30(19)	1.68(35)

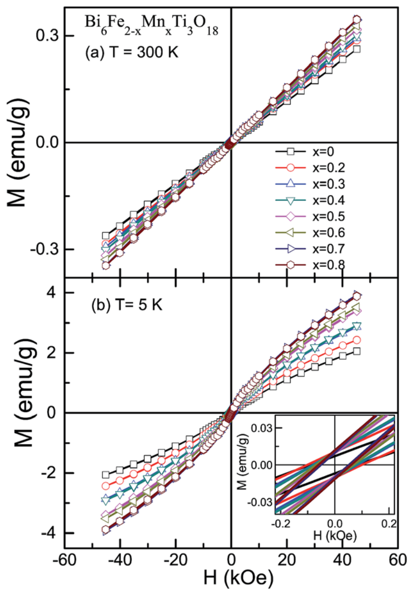

Fig. 4 Field dependence of magnetization of $Bi_6Fe_{2-x}Mn_xTi_3O_{18}$ ($0 \leq x \leq 0.8$) at (a) 300 K and (b) 5 K. The inset of (b) is the enlarged view of the loops under the low field range at 5 K.

indicates stronger AFM interactions between Fe and Mn spins. We found that the M–H plots of BFMTO can be well fitted by the modified Brillouin function, as shown in Fig. 5. The fitting values of M_S are displayed in Table 1, which show an identical tendency to those of the μ_{eff} obtained from the modified Curie–Weiss law in Table 1, *i.e.*, it increases upon increasing the doping level of Mn from 0 to 0.7 and then drops with a further increase in x to 0.8. Moreover, the values of T_0 decrease monotonously upon increasing the doping level of Mn, implying the weakening of AFM interactions with the increase in x, which is in good agreement with the variation in Curie–Weiss temperature shown in Table 1. Therefore, the magnetic behavior of BFMTO can be well explained by the modified Curie–Weiss relation and the modified Brillouin function.

The temperature dependence of the dielectric constant ε' and the loss tangent tan δ at different frequencies from 300 to 1000 K are shown in Fig. 6 and 7, and Fig. 8 and 9, respectively. For BFTO (Fig. 6(a)), the ε'–T plots display a bump shoulder and an abrupt hump at around 590 K and 965 K, respectively. The location of the hump is the characteristic temperature (T_c) of the ferroelectric transition.[26] For the samples where $x = 0.2$, 0.3, and 0.4 (Fig. 6(b)–(d)), the dielectric constants exhibit a similar behavior. The dielectric constant increases slowly and shows an abrupt increase above 800 K corresponding to the peak temperature of the loss tangent. Moreover, the location of the peak shifts toward a higher temperature with increasing frequency, especially for the samples with $x = 0.3$ (Fig. 8(c)) and $x = 0.4$ (Fig. 8(d)). The frequency dispersion of the dielectric constant and the frequency dependence of the loss peak are

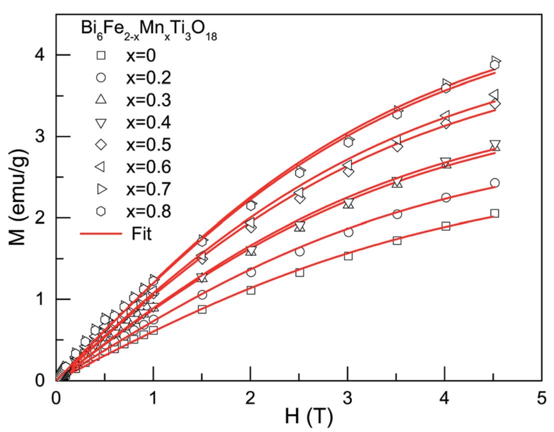

Fig. 5 M *vs.* H curves at 5 K. The solid lines are the fit data according to the modified Brillouin function.

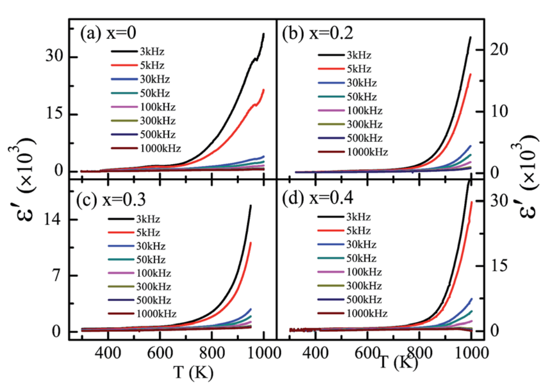

Fig. 6 Temperature dependence of dielectric constant at the frequency of 3, 5, 30, 50, 100, 300, 500, and 1000 kHz for $Bi_6Fe_{2-x}Mn_xTi_3O_{18}$ with (a) $x = 0$, (b) $x = 0.2$, (c) $x = 0.3$, and (d) $x = 0.4$.

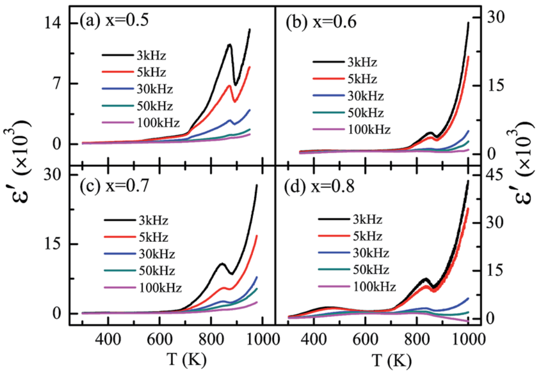

Fig. 7 Temperature dependence of dielectric constant at the frequency of 3, 5, 30, 50, and 100 kHz for $Bi_6Fe_{2-x}Mn_xTi_3O_{18}$ with (a) $x = 0.5$, (b) $x = 0.6$, (c) $x = 0.7$, (d) $x = 0.8$.

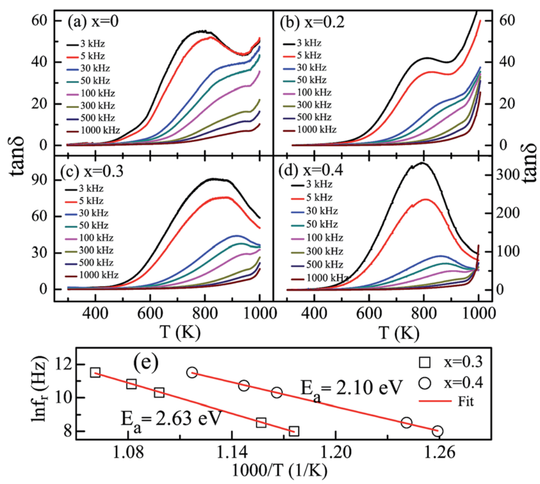

Fig. 8 Temperature dependence of dielectric loss at the frequency of 3, 5, 30, 50, 100, 300, 500, and 1000 kHz for $Bi_6Fe_{2-x}Mn_xTi_3O_{18}$ with (a) $x = 0$, (b) $x = 0.2$, (c) $x = 0.3$, (d) $x = 0.4$, and (e) Arrhenius plot of relaxation frequency *versus* temperature for the samples with $x = 0.3$ and $x = 0.4$.

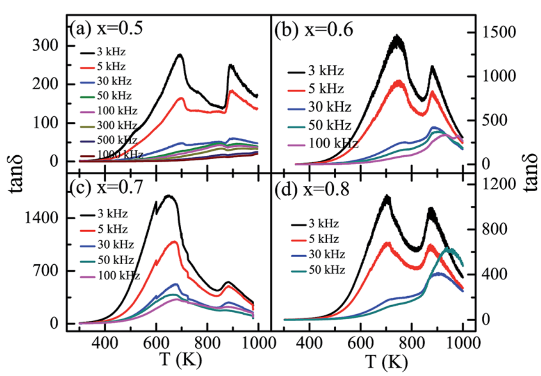

Fig. 9 Temperature dependence of dielectric loss at different frequencies for $Bi_6Fe_{2-x}Mn_xTi_3O_{18}$ with (a) $x = 0.5$, (b) $x = 0.6$, (c) $x = 0.7$, (d) $x = 0.8$.

characteristics of the dielectric relaxation,[27–29] and can be ascribed to a thermally activated process. If so, the characteristic relaxation frequency f_r (the frequency peak in the dielectric loss spectra) should obey the Arrhenius law: $f_r = f_\infty \exp(-E_a/k_BT)$, where f_∞ denotes the frequency at infinite temperature, E_a the activation energy, and k_B denotes the Boltzmann constant. The experimental data can be well described according to the Arrhenius law (Fig. 8(e)), and the activation energy E_a is 2.63 eV and 2.10 eV for the $x = 0.3$ and $x = 0.4$ samples, respectively. These values are close to 2.62 eV in $Bi_6FeCoTi_3O_{18}$,[30] and 2.72 eV in $Bi_6Fe_2Ti_{2.8}Nb_{0.1}Co_{0.1}O_{18}$.[31] The values of E_a are much larger than those due to the oxygen vacancies in oxide ceramics, *e.g.*, 0.87 eV in $Bi_4Ti_3O_{12}$,[32] 0.74–0.86 eV in Bi:$SrTiO_3$ solid solutions,[33] and 1.206 eV in $Bi_6Fe_2Ti_3O_{18}$ thin film.[34] This inconsistency implies that the relaxation mechanism for the dielectric loss peak may be not related to the thermal motion of oxygen vacancies in the bulk. For the samples with $x \geq 0.5$, there is a peak in the dielectric constant spectra, as shown in Fig. 7(a)–(d), and the peak temperature does not change with the frequency, which is characteristic of a paraelectric–ferroelectric phase transition. T_c can be determined to be 872 K ($x = 0.5$), 853 K ($x = 0.6$), 841 K ($x = 0.7$), and 835 K ($x = 0.8$). Moreover, the dielectric loss peak (Fig. 9(a)–(d)) is observed at around T_c and it normally appears at the temperatures at which the dielectric constant varies remarkably.

4 Conclusions

In summary, we have studied the structural, magnetic, and dielectric properties of Aurivillius phase $Bi_6Fe_{2-x}Mn_xTi_3O_{18}$ ($0 \leq x \leq 0.8$). The magnetic properties of all samples can be understood by a dominant paramagnetic state with the presence of short-range antiferromagnetic interactions and a weak ferromagnetic ordering. The dielectric loss of $Bi_6Fe_{1.7}Mn_{0.3}Ti_3O_{18}$ and $Bi_6Fe_{1.6}Mn_{0.4}Ti_3O_{18}$ exhibits a thermally activated relaxation process, and the activation energy is 2.63 eV and 2.10 eV for the samples with $x = 0.3$ and 0.4, respectively. The $0.5 \leq x \leq 0.8$ samples exhibit a paraelectric–ferroelectric phase transition.

Acknowledgements

This work was supported by the National Natural Science Foundation of China (Grant no. 11274313 and 11374304), the Anhui Provincial Natural Science Foundation (Grant no. 1208085MA06), and the Joint Funds of the National Natural Science Foundation of China and the Chinese Academy of Sciences' Large-Scale Scientific Facility (Grant no. U1232138 and U1232210). It was also sponsored by the Scientific Research Foundation for the Returned Overseas Chinese Scholars, State Education Ministry. The author Y. P. Sun acknowledges support by the National Key Basic Research (Grant no. 2011CBA00111).

References

1 W. Eerenstein, N. D. Mathur and J. F. Scott, *Nature*, 2006, **442**, 759–765.

2 S.-W. Cheong and M. Mostovoy, *Nat. Mater.*, 2007, **6**, 13–20.
3 R. Ramesh and N. A. Spaldin, *Nat. Mater.*, 2007, **6**, 21–29.
4 B. Aurivillius, *Ark. Kemi*, 1949, **1**, 463.
5 B. Aurivillius, *Ark. Kemi*, 1949, **1**, 499.
6 X. Mao, W. Wang, X. Chen and Y. Lu, *Appl. Phys. Lett.*, 2009, **95**, 082901.
7 A. T. Giddings, M. C. Stennett, D. P. Reid, E. E. McCabe, C. Greaves and N. C. Hyatt, *J. Solid State Chem.*, 2011, **184**, 252–263.
8 C. H. Wang, Z. F. Liu, L. Yu, Z. M. Tian and S. L. Yuan, *Mater. Sci. Eng., B*, 2011, **176**, 1243–1246.
9 B. H. Park, B. S. Kang, S. D. Bu, T. W. Noh, J. Lee and W. Jo, *Nature*, 1999, **401**, 682–684.
10 X. W. Dong, K. F. Wang, J. G. Wan, J. S. Zhu and J.-M. Liu, *J. Appl. Phys.*, 2008, **103**, 094101.
11 H. Sun, X. Lu, J. Su, T. Xu, C. Ju, F. Huang and J. Zhu, *J. Phys. D: Appl. Phys.*, 2012, **45**, 385001.
12 J. Yang, L. H. Yin, D. F. Shao, X. B. Zhu, J. M. Dai and Y. P. Sun, *Europhys. Lett.*, 2011, **96**, 67006.
13 L. Keeney, S. Kulkarni, N. Deepak, M. Schmidt, N. Petkov, P. F. Zhang, S. Cavill, S. Roy, M. E. Pemble and R. W. Whatmore, *J. Appl. Phys.*, 2012, **112**, 052010.
14 L. Keeney, T. Maity, M. Schmidt, A. Amann, N. Deepak, N. Petkov, S. Roy, M. E. Pemble, R. W. Whatmore and D. Johnson, *J. Am. Ceram. Soc.*, 2013, **96**, 2339–2357.
15 J. B. Goodenough, *J. Phys. Chem. Solids*, 1958, **6**, 287–297.
16 J. Kanamori, *J. Phys. Chem. Solids*, 1959, **10**, 87–98.
17 M.-F. Lin, V. K. Thakur, E. J. Tan and P. S. Lee, *J. Mater. Chem.*, 2011, **21**, 16500–16504.
18 M.-F. Lin, V. K. Thakur, E. J. Tan and P. S. Lee, *RSC Adv.*, 2011, **1**, 576–578.
19 J. Yang, W. Tong, Z. Liu, X. B. Zhu, J. M. Dai, W. H. Song, Z. R. Yang and Y. P. Sun, *Phys. Rev. B: Condens. Matter Mater. Phys.*, 2012, **86**, 104410.
20 Z. Liu, J. Yang, X. W. Tang, L. H. Yin, X. B. Zhu, J. M. Dai and Y. P. Sun, *Appl. Phys. Lett.*, 2012, **101**, 122402.
21 A. Punnoose, J. Hays, A. Thurber, M. H. Engelhard, R. K. Kukkadapu, C. Wang, V. Shutthanandan and S. Thevuthasan, *Phys. Rev. B: Condens. Matter Mater. Phys.*, 2005, **72**, 054402.
22 E. Jartych, T. Pikula, M. Mazurek, A. Lisinska-Czekaj, D. Czekaj, K. Gaska, J. Przewoznik, C. Kapusta and Z. Surowiec, *J. Magn. Magn. Mater.*, 2013, **342**, 27–34.
23 I. Dzyaloshinsky, *J. Phys. Chem. Solids*, 1958, **4**, 241–255.
24 T. Moriya, *Phys. Rev.*, 1960, **120**, 91–98.
25 I. A. Sergienko and E. Dagotto, *Phys. Rev. B: Condens. Matter Mater. Phys.*, 2006, **73**, 094434.
26 J. B. Li, Y. P. Huang, G. H. Rao, G. Y. Liu, J. Luo, J. R. Chen and J. K. Liang, *Appl. Phys. Lett.*, 2010, **96**, 222903.
27 A. Srinivas, D. W. Kim, K. S. Hong and S. V. Suryanarayana, *Appl. Phys. Lett.*, 2003, **83**, 2217.
28 V. K. Thakur, E. J. Tan, M.-F. Lin and P. S. Lee, *J. Mater. Chem.*, 2011, **21**, 3751–3759.
29 V. K. Thakur, M.-F. Lin, E. J. Tan and P. S. Lee, *J. Mater. Chem.*, 2012, **22**, 5951–5959.
30 J. Yang, L. H. Yin, Z. Liu, X. B. Zhu, W. H. Song, J. M. Dai, Z. R. Yang and Y. P. Sun, *Appl. Phys. Lett.*, 2012, **101**, 012402.
31 B. Yuan, J. Yang, J. Chen, X. Z. Zuo, L. H. Yin, X. W. Tang, X. B. Zhu, J. M. Dai, W. H. Song and Y. P. Sun, *Appl. Phys. Lett.*, 2014, **104**, 062413.
32 H. S. Shulman, D. Damjanovic and N. Setter, *J. Am. Ceram. Soc.*, 2000, **83**, 528–532.
33 C. Ang, Z. Yu and L. E. Cross, *Phys. Rev. B: Condens. Matter Mater. Phys.*, 2000, **62**, 228.
34 W. Bai, G. Chen, J. Y. Zhu, J. Yang, T. Lin, X. J. Meng, X. D. Tang, C. G. Duan and J. H. Chu, *Appl. Phys. Lett.*, 2012, **100**, 082902.